Sedimentary Geology 347 (2017) 67–78

Contents lists available at ScienceDirect

Sedimentary Geology

journal homepage: www.elsevier.com/locate/sedgeo

Desiccation cracks in siliciclastic deposits: Microbial mat-related compared to abiotic sedimentary origin

Olga Kovalchuk [a,*], George W. Owttrim [b], Kurt O. Konhauser [a], Murray K. Gingras [a]

[a] Department of Earth and Atmospheric Sciences, University of Alberta, Edmonton, Alberta T6G 2E3, Canada
[b] Department of Biological Sciences, University of Alberta, Edmonton, Alberta T6G 2E9, Canada

ARTICLE INFO

Article history:
Received 20 July 2016
Received in revised form 4 November 2016
Accepted 6 November 2016
Available online 10 November 2016

Editor: Dr. B. Jones

Keywords:
Microbial mat
Desiccation cracks
Crack pattern
Siliciclastic sediment
Mat-related structures
Experimental desiccation

ABSTRACT

Siliciclastic sediment colonized by microbial mats yield a set of distinct sedimentary fabrics that are collectively called "mat-related structures (MRS)". In the rock record, versatile cracks are observed in biostabilized strata, but the mechanisms responsible for their formation remain debated. Microbially stabilized sediments produce desiccation cracks that serve as modern analogs for fossil microbial cracks. However, since both microbial mat shrinkage and clay shrinkage may contribute to the formation of these desiccation cracks, it is difficult to isolate the influence of the microbial mat on the resulting crack formation, distribution and morphology. To address this issue, we conducted a series of desiccation experiments that determine differences between microbially influenced desiccation cracks (i.e. biotic) and those formed in identical, but sterilized (i.e. abiotic) siliciclastic sediment. Three sediment mixtures were used: (1) very fine-sized sand, (2) mixed (ungraded) silt/clay, and (3) normally graded silt/clay. In all of the experiments, the water-rich microbial mat contracted substantially while drying, producing isolated pockets of shallow, but wide cracks, the distribution of which was controlled by heterogeneities in the mat structure and thickness variations of the mat. In the clay-poor substratum, the microbial mat was the only crack-forming mechanism, while in the clay-rich substrata (experiments 2 and 3) desiccation cracks were more strongly influenced by clay shrinkage. The abiotic clay-rich sediment produced a polygonal network of deep cracks intersecting at 90–120° junctions. In the biotic clay-rich experiments, the microbial mat modified these desiccation features by withstanding crack propagation or by producing curled-up crack polygon margins. Even though a microbial mat shrinks substantially with desiccation, its cohesive nature and heterogeneous distribution prevents the formation of a regular crack network, but its shallow penetration into the sediment limits its influence on cracking. The biotic crack formation is best characterized by a heterogeneous distribution of wide, but shallow pockets of radiating cracks that do not connect to one another, while abiotic cracking is best characterized by an orthogonal network of deep, intersecting cracks. By comparing biotic and abiotic shrinkage cracks formed in identical sediment, we improve our understanding of modern desiccation features and thus strengthen our interpretation of the rock record.

1. Introduction

Loose siliciclastic sediment becomes biostabilized once it is colonized by a microbial mat. During biostabilization, cyanobacterial filaments entangle sedimentary grains, and extracellular polymeric substances (EPS) secure grains into a cohesive matrix, protecting the bound grains from hydraulic entrainment and subsequent transport (De Boer, 1981; Hagadorn and McDowell, 2012). EPS are hydrated polymer chains, approximately 99% water by weight, which are secreted by the microorganisms and play a key role in their survivability (Decho, 1990). Microbial mats (i.e. biomats *sensu* Krumbein, 1983; Krumbein et al., 2003) are thus sheet-like structures composed of diverse microbial communities, EPS and entrapped sedimentary grains (for review of proposed definitions see Gerdes, 2010). Owing to their high cohesiveness, tensile strength and erosional resistance, biomats facilitate exceptional preservation of sedimentary structures, trace fossils and soft tissues (Gehling, 1999; Seilacher, 2008; Gingras et al., 2011; Carmona et al., 2012; Pecoits et al., 2012).

In binding the siliciclastic sediment, biomats leave distinctive structures and micro-impressions, collectively referred to as mat-related structures (MRS) (Schieber et al., 2007). Ubiquitous MRS are described from the siliciclastic rock record throughout the geologic time, but especially in Precambrian through to Ordovician strata, when microbial mats thrived in a wide range of environments (Schieber, 1998; Seilacher, 1999; Noffke et al., 2006a, 2006b; Sarkar et al., 2006, 2008; Porada and Druschel, 2010; Noffke et al., 2013 and others). An assortment of mat-related structures have been documented from modern-day tidal

* Corresponding author.
E-mail addresses: okovalch@ualberta.ca (O. Kovalchuk), gowttrim@ualberta.ca (G.W. Owttrim), kurtk@ualberta.ca (K.O. Konhauser), mgingras@ualberta.ca (M.K. Gingras).

http://dx.doi.org/10.1016/j.sedgeo.2016.11.002
0037-0738/

flats, lagoons and sabkhas (Cameron et al., 1985; Noffke, 1998, 1999 and others). While some modern MRS bear a striking resemblance to the structures seen in the rock record, many fossil structures that are thought to be related to biostabilization do not have clear modern analogs (Dornbos et al., 2007; Eriksson et al., 2007a; Bouougri and Porada, 2007; Bottjer and Hagadorn, 2007; Porada et al., 2008).

One puzzling category of fossil MRS is microbial shrinkage cracks. In Precambrian through to Ordovician rocks, cracks of various morphologies and sizes reoccur on bedding planes in siliciclastic strata, ranging from isolated spindle shaped, sinuous cracks, to triradiate morphologies and complex polygonal networks (Porada and Loeffler, 2000; Bouougri and Porada, 2002; Parizot et al., 2005; Harazim et al., 2013). Proximity of such cracks to microbial fabrics, carbonaceous wavy-crinkly laminae, and the presence of authigenic pyrite suggests that the bedding planes were once biostabilized and that the cracks were (at least in part) associated with biomats. Fossil cracks found in clean sand are the most convincing evidence of microbial influence, because rigid sand grains do not contract and also lack cohesiveness to form cracks (Eriksson et al., 2007a). The leading interpretation is that such fossil cracks form by subaerially exposed and desiccating microbial mats, such as those observed in the modern intertidal and supratidal biostabilized sediments (Cameron et al., 1985; Gerdes et al., 1993; Gerdes, 2000; Eriksson et al., 2007a; Gerdes, 2007; Bose and Chafetz, 2009; Cuadrado et al., 2014). Since tidal flats are typically characterized by the presence of silt and clay deposited during fair conditions, the microbial cracks are the result of both biomat and clay shrinkage, producing an irregular

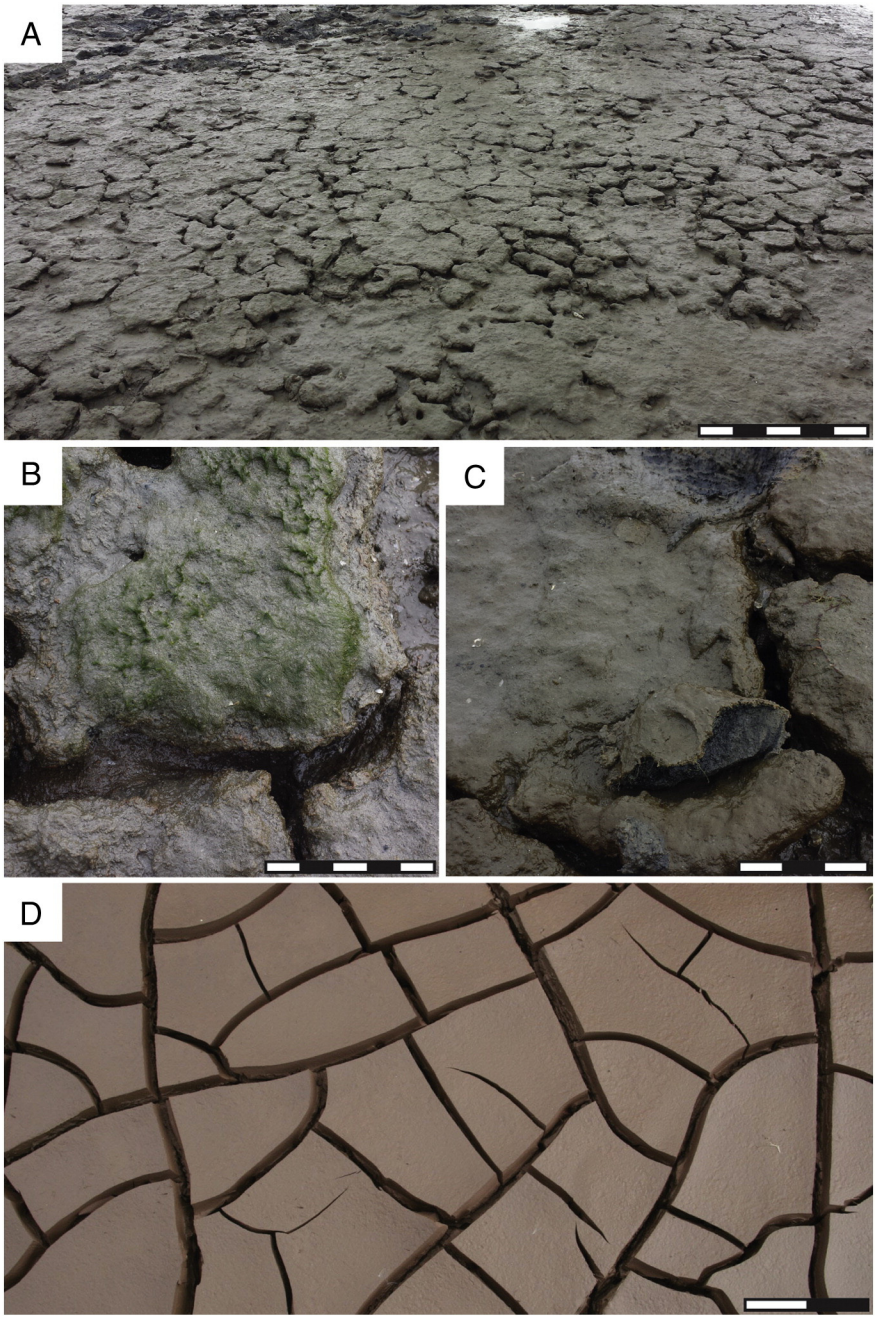

Fig. 1. Desiccation cracks observed in biostabilized (A–C) and predominantly abiotic (D) sediments. (A) Desiccation cracks observed in clay-rich sediment colonized by a microbial mat, Fraser River delta, British Columbia. The cracks intersect to form irregular polygons with rounded edges that vary in size 3–40 cm. Microbial mat prevents the features from getting destroyed with flooding, although some polygons are eroded, forming wide depressions. Scale bar is 50 cm. (B) Motile cyanobacterial filaments forming a reticulate pattern above the sediment. Scale bar is 5 cm. (C) Cross-section of the biomat, showing a thin 1-2 mm layer of photosynthetic bacteria and a dark anoxic zone underneath the mat. Scale bar is 3 cm. (D) Orthogonal cracking pattern, typical of a desiccated clay-rich sediment, observed on the shores of Petitcodiac River, New Brunswick. Scale bar is 20 cm.

network that is distinct from the orthogonal pattern induced by clay desiccation (Fig. 1).

It is difficult to isolate microbial mat influence on crack development and morphology in intertidal and supratidal regions, because the observed microbial cracks have a complex history of formation. The desiccation is driven by tidal water table fluctuations causing multiple desiccation and biostabilization cycles during which the pore pressure variations may drive the underlying sediment to infill the cracks or produce petee structures which can serve as loci of cracks (Porada et al., 2007). Evaporation is typically the final step in removing interstitial water and producing desiccation cracks. The goal of this study was thus to determine microbial influence on crack development and morphology by providing a direct comparison of microbial mat- and sediment-related desiccation cracks formed during a single evaporation event. Since desiccation in our experiments is driven by evaporation only, the results are most directly comparable to structures produced in temporary pools in supratidal and terrestrial environments. Nonetheless, these findings can also be used as a basis for understanding desiccation in more complex tidal settings and extrapolated to the rock record.

2. Methods

2.1. Preparation of substratum

Siliciclastic sediment was collected at the Fraser River Delta near Vancouver, Canada, and then used as the substrata for the experiments. The sediment was rinsed and then heated in a convection oven at 110 °C for 24 h, drying and sterilizing the sediment. The dry sediment was manually disaggregated using a mortar and pestle and then sieved for 10 min using W.S. Tyler RX-29 automatic sieve shaker. Sediments collected in sieves No. 120–230 (125–62 μm) were washed with distilled water to reduce the number of residual fines and to produce a sediment dominated by sand-sized grains. Sediments finer then coarse silt (<62 μm) were collected in the bottom pan and used as the silt/clay substratum: this fraction was further analyzed using a Micromeritics Corporation Sedigraph 5100, which determined 18–25 wt% clay content (i.e. phylosillicates < 2–4 μm in diameter) (Fig. 2).

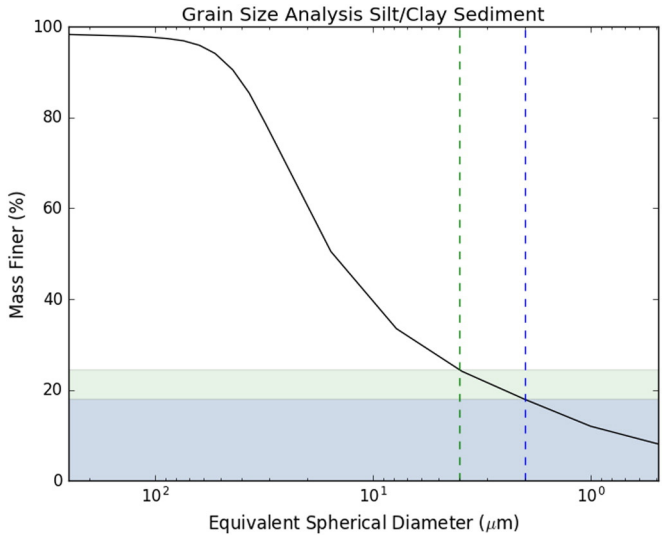

Fig. 2. Grain size distribution in mixed (ungraded) and normally graded silt/clay sediment. Clay content ranges from 18 to 25% of the bulk composition, depending if using 2 μm or 4 μm as the silt/clay cut-off.

2.2. Preparation of tanks

Six glass tanks, with dimensions of 30 × 30 × 15 cm, were constructed. Tanks were filled with an even 2 cm layer of sediment and paired in the following way: tank-pair 1 was filled with very fine sand (125–62 μm), tank-pair 2 with mixed (ungraded) silt/clay (<62 μm), and tank-pair 3 with normally graded silt/clay (<62 μm) (clay-rich top layer and a silt-rich bottom layer). For each tank-pair, one tank was inoculated with cyanobacteria and left to form a microbial mat over a period of 35 days, whereas the other tank was exposed to daily UV-C irradiation to sterilize the sediment and maintain abiotic conditions. Dechlorinated, nutrient spiked tap water and deionized type 1 (ultrapure) water was used for the biotic and abiotic tanks, respectively. The water was slowly siphoned into each of the tanks to prevent resorting of the sediment, except for the normally graded tank, where sediment was stirred and allowed to naturally settle from suspension. During the desiccation experiments, water was left to evaporate naturally in the tanks, and repeated UV-C irradiation kept one tank of each pair sterile throughout desiccation.

2.3. Inoculation and growth of cyanobacteria (biotic tank)

Cultures of non-axenic filamentous cyanobacterium *Leptolyngbya* sp. CPCC 696 (Canadian Phycological Culture Centre: CPCC) were used to establish the biomats in this study. *Leptolyngbya* were maintained on BG-11 agar plates and inocula grown in liquid BG-11 at 30 °C under a light intensity of 30 μE/m^2/s (Owttrim, 2012). The tanks were filled with dechlorinated tap water (such as that used in fresh water aquariums, using Seachem Prime Water Conditioner) (Hagadorn and McDowell, 2012), containing dissolved plant fertilizer (Schultz African Violet Liquid Plant Food, 8-14-9, 7 drops/L of water) to which a liquid *Leptolyngbya* culture was introduced. Tank water level was maintained at 3–4 cm above the substrate. The microbial biofilms developed into cohesive microbial mats over a period of 35 days, reaching a thickness of approximately 1 mm while wet.

2.4. Sterilization of sediment (abiotic tank)

The sterilized tanks were filled with 3–4 cm type 1 purified water from a Barnstead™ Easypure™ II Water Treatment System. Using two Philips 15 W mercury-vapor germicidal lamps, the abiotic tanks were subjected to UV-C irradiation for 30 min daily. The UV-C spectrum peaked at 254 nm with 80 μW/cm^2 power output (averaged over the UV-C band: 100 nm–290 nm wavelengths) at the water's surface.

2.5. Desiccation experiment

Starting with equal water levels, the biotic and abiotic tanks were left to desiccate *via* evaporation at room temperature (20–22 °C). Desiccation took one week to complete. Observations were recorded daily, focusing on differences between crack formations in abiotic versus biomat colonized sediments, specifically the timing of first desiccation crack formation and increases in the density or sizes of the cracks with time. Daily photographs were taken using Canon EOS 50D digital SLR camera placed on a photo stand directly above the tanks. Macro-lens was used to take more detailed photographs of the desiccation features.

In order to quantify the produced crack polygons in the clay-rich sediments, the photographs were converted into gray scale images, following a conversion into binary images, where the black pixels represent cracks and the white pixels represent polygons. Crack trajectories in the binary images were corrected and stray pixels were deleted, by overlying the binary image with the original photograph. Photograph processing algorithms were applied to the binary image using Python's Skimage library, which identified polygons (white pixels) using the bounding cracks (black pixels). The polygon surface areas were calculated, first based on how many pixels each contained and later converted

to cm^2. In order to exclude small features that were not representative of the desiccation network, 1 cm^2 filter was applied.

Additionally, the dry samples from each tank were analyzed with a Scanning Electron Microscope (SEM) to observe the bacterial and EPS interactions with the sediment grains. SEM micrographs were taken to document these findings.

3. Results

3.1. Microbial growth and development into a mat

In all of the biotic tank experiments, a visible biofilm formed on the sediment within 48 h of inoculation. The bacteria first organized themselves into small conical tufts, which then developed into a stringy reticulate pattern as the biofilm matured: this is similar to the growth patterns described in Shepard and Sumner (2010). Development of a microbial mat was accompanied by the production of metabolic gases which were trapped underneath the mat, within the mat fabric, and by the bacterial mucilage water, forming bubbles (Fig. 3). Some small gas bubbles, 1–3 mm in diameter, were stable and remained present throughout the mat's lifecycle, while others coalesced into bigger gas domes that were often released into the atmosphere (e.g. Bosak et al., 2010).

3.1.1. Sand substratum

The microbial mat effectively biostabilized the sand substratum, forming a 1 mm thick, cohesive layer that was flat-laying against the sediment (Fig. 3A, B). SEM analysis shows that bacterial filaments and EPS penetrate into the sand using the pore space, reinforcing attachment to the substrate (Fig. 9B). Gas bubbles were observed escaping the mat surface, but they did not cause the mat to become buoyant due to strong attachment of the mat to the substrate.

3.1.2. Silt/clay substratum

The microbial mat was less successful in biostabilizing the clay-rich substratum and it tended to become suspended in the water column by accumulated metabolic gases forming domal structures (Fig. 3C, D). SEM images show that bacterial filaments and EPS did not penetrate as deeply into the clay-rich substratum due to smaller pore sizes, resulting in a weak attachment (Fig. 9E). Notable wrinkles were developed in the microbial mat, initially at the slopes of the suspended mat-dome structure, but later over the entire biomat as the domes collapsed due to release of gas (Fig. 3D). The mat did not cover the entire surface area of the tank and mainly concentrated at the center due to suspension and buckling. A new biofilm started to form in the available space at the edges of the tank. The old mat became scared by the escaping gas bubbles giving it a perforated texture (Fig. 3D).

3.2. Microbial mat desiccation on sandy versus clay-rich substrata

Growth of the microbial mat, in terms of its lateral and vertical colonization of the substrata, had a direct influence on the desiccation patterns. Only the thin layer of sediment that was colonized by the cyanobacteria (up to 500 μm in the sand and only about 150 μm in the clay-rich sediment) was involved in the biomat-induced desiccation, resulting in shallow cracks. Imperfections in the biomat led to structural weaknesses, such as gas domes and tears, that provided the loci for radiating cracks. By contrast, regions of greater biomat thickness prevented cracks from propagating and connecting to one another. Table 1 summarizes the crack patterns formed in the biotic and abiotic substrata.

3.2.1. Sand substratum

In the sand substratum, shrinkage of the biomat was the only mechanism that formed desiccation cracks. Initial cracking and coiling of the margins occurred rapidly, but the biomat and attached sediment continued to shrink and curl upwards over the following 24 h (Fig. 4A–C). Desiccation resulted in uneven crack network over the bed surface. Large portions of the biomat, for example, at the bottom left corner of the tank, remained intact, although the biomat displayed an overall contraction (reduction in surface area) (Fig. 4C). Weaknesses in the biomat, such as scarring by the escaping and trapped gas bubbles, provided loci for crack initiation.

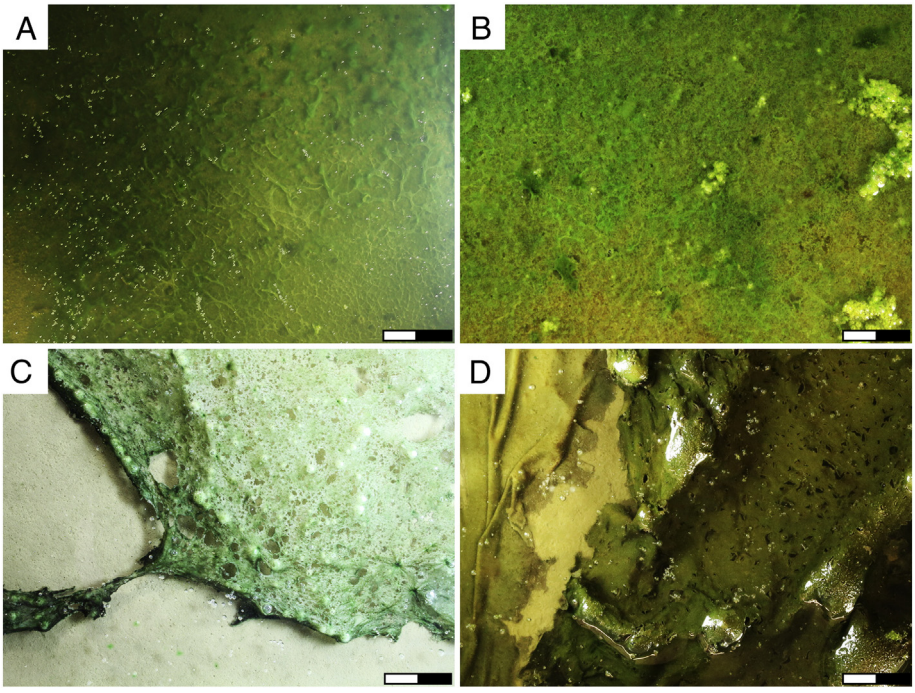

Fig. 3. Microbial mat growth and development. (A) 10 day old biofilm forming a reticulate surface pattern on the very fine sand substratum, note the small gas bubbles trapped at the water surface. (B) 30 day old microbial mat developed on the very fine sand substratum showing a more complex reticulate pattern. (C) Normally graded silt/clay sediment colonized with a 7 day old biofilm showing gas bubbles that are accumulating underneath the biofilm. (D) 30 day old microbial mat developed on the mixed (ungraded) silt/clay substratum. Microbial mat becomes wrinkled and torn due to escape of gases. Scale bar is 2 cm.

Table 1
Summary of desiccation features produced in biotic and abiotic sediments.

	Biotic	Abiotic
Very fine sand	Underlying sediment (sub-sediment): No cracking. Mat: Radiating, shallow, wide, composite cracks up to 7 cm wide, consisting of microbial mat and attached sediment. The crack margins are coiled up to 360°, forming detached curls.	Rare, isolated, thin (hair-like) cracks.
Silt/Clay (ungraded, mixed)	Underlying Sediment (sub-sediment): Flat-laying polygons separated by deep cracks up to 7 mm wide, intersecting in 90–120° junctions. Rare tapering cracks forming incomplete polygons. Mat: Top thin layer, consisting of the mat and attached sediment, produced coiling of the clay-induced crack margins. The mat curls detached from the sub-sediment below and coiled 180-360°. Also, shallow radiating cracks with coiled margins formed independently of the cracked clay-rich sediment below.	Flat-laying polygons separated by deep cracks up to 7 mm wide, intersecting in 90–120° junctions. Rare smaller shallow cracks forming incomplete polygons.
Silt/Clay (normally graded)	Underlying Sediment (sub-sediment): Concave-up polygons separated by deep cracks up to 2 cm wide, intersecting in 90–120° junctions. Rare tapering cracks forming incomplete polygons. Mat: Top thin layer, consisting of the mat and attached sediment, produced coiling of the clay-induced crack margins. The mat curls detached from the sub-sediment below and coiled up to 180°. Also, shallow radiating cracks with coiled margins originated from drying of uplifted gas domes and were independent of the cracked clay-rich sediment below.	Detached concave-up polygons separated by cracks up to 2 cm wide, intersecting in 90–120° junctions. Rare smaller shallow cracks forming incomplete polygons.

The desiccated biostabilized sand did not show typical mud crack morphologies, such as polygons, which are completely separated from each other by a rectilinear network of deep cracks. Instead, shallow, radiating cracks that did not propagate far from their point of origin were often isolated from one another or connected to form pockets of composite cracks. Curling at the crack margins obscured the initial crack pattern and produced wide cracks that exposed the sub-sediment underneath that showed no evidence of cracking (Fig. 4B, C).

The desiccated abiotic sand of identical composition produced two straight, thin (hair-like) cracks (Fig. 4D), no other contractional features were observed in this abiotic sediment.

3.2.2. Silt/clay mixed (ungraded) substratum

In the clay-rich sediment, both the clay and the biomat shrinkage contributed to the formation of the desiccation cracks (Fig. 5A–C). The clay sub-sediment cracked first while the biomat cover was too moist to crack (Fig. 5B). Initial dilation of the clay-induced cracks was rapid, but propagation and widening of the cracks occurred over a 24-hour period. Continuous straight to gently curved cracks penetrated the entire depth of the substratum (except for the top biostabilized layer) and generally intersected in 90–120° junctions, forming square and pentagonal polygons. Also, a few rare and shallow tapering cracks produced incomplete polygons. The crack widths reached up to 7 mm (Fig. 5C).

At the time of clay desiccation, the biomat remained moist and was either torn by the cracks or was stretched across a crack (bridging the crack) (Fig. 5B). Approximately 24 h after first appearance of cracks in the clay-rich sub-sediment, the biomat dried and curled upwards along the previously developed crack margins, although a few clay-induced cracks remained bridged by the biomat, even after drying (Fig. 5C, black arrows). Shallow, wide cracks with coiled margins, similar to those observed in the sand, developed where there were weaknesses in the biomat structure due to gas escape.

Cracks in the abiotic mixed silt/clay substratum were similar to those formed in the biostabilized counterpart. Abiotic cracks penetrated the entire depth of the substratum forming square and pentagonal polygons, with a few smaller shallow cracks forming incomplete polygons (Fig. 5D). Quantitatively comparing the crack bounded polygon surface areas, however, revealed that the mean polygon surface area was larger in the biotic sediment (28.6 cm^2) as compared to the abiotic sediment (19.3 cm^2). Furthermore, less polygons formed the biotic sediment ($n = 26$) as compared to the abiotic counterpart ($n = 40$) (Fig. 7A-C).

3.2.3. Silt/clay normally graded substratum

Similar to the mixed (ungraded) silt/clay experiment, the normally graded sub-sediment beneath the biomat cracked first, thereby controlling the ensuing cracking pattern and tearing the still moist biomat (Fig. 6A, B). Desiccation of the normally graded clay-rich sub-sediment, produces concave-up crack polygons. When the biomat became dry, 24 h after the initiation of clay-induced cracking, it and the attached layer of sediment curled upwards along the existing crack polygon margins, while some of the clay- induced cracks remained bridged by the dry biomat (Fig. 6C).

During dessication of the abiotic and normally graded silt/clay substratum, concave-up polygons with raised margins formed that were separated by deep cracks (Fig. 6D). These structures were similar to those formed by the clay-rich sub-sediment in the biotic tank. The concave-up nature of the polygons produced wide crack separations, up to 2 cm, which is much wider than observed in the mixed silt/clay sediment. As with the mixed silt/clay experiment, the mean crack polygon surface area was larger in the biotic sediment (37.3 cm^2) as compared to the abiotic sediment (31.2 cm^2), and less polygons were observed in the biotic sediment (18) as compared to the abiotic counterpart (24) (Fig. 7D–E).

3.3. Textures produced by desiccation

The thickness of the siliciclastic layer that was colonized by the biomat varied laterally, resulting in uneven desiccated mat curl structure. This differential attachment of grains to the biomat bestowed a pitted and rugose texture to the underside of the biomat curls and on the sub-sediment surface (Fig. 8). The texture was more prominent in the mixed clay/silt substratum (Fig. 8C, D) than in the sand (Fig. 8A, B), and it was not visible in the normally graded silt/clay substratum.

3.4. SEM imaging

Dry mat curls which formed in the biostabilized very fine sand and mixed (ungraded) silt/clay were analyzed under SEM. In plan view,

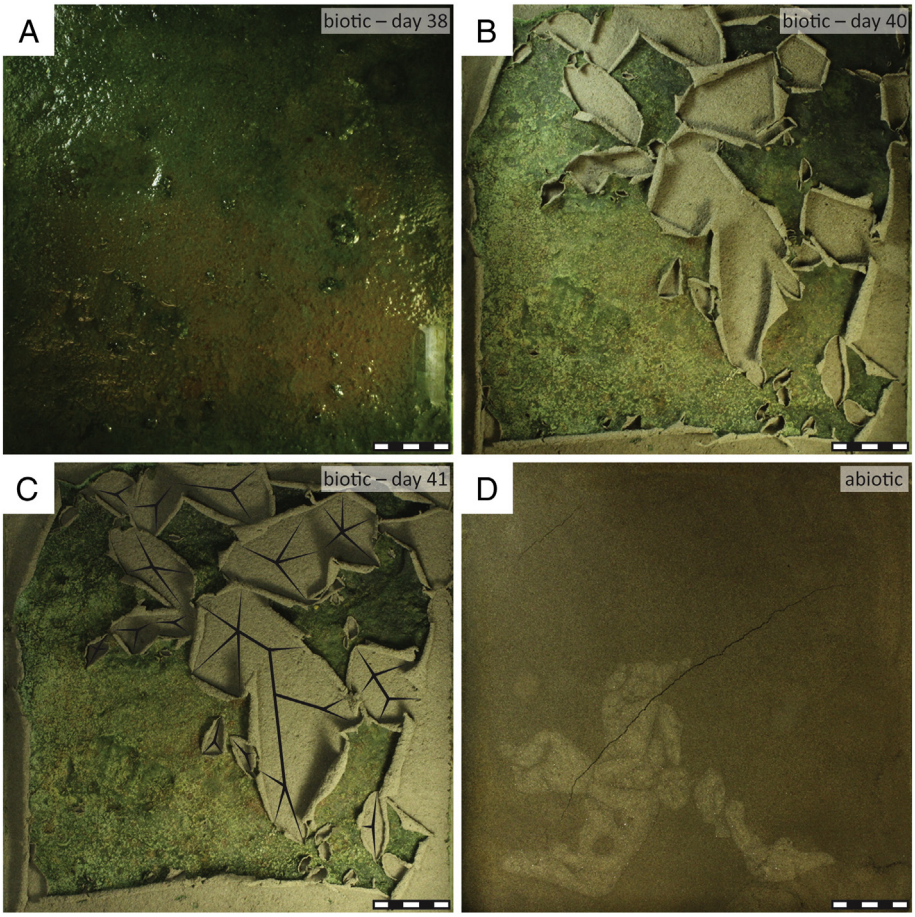

Fig. 4. Progressive desiccation of the biomat colonized very fine sand (A–C) and desiccated abiotic very fine sand substrata (D). (A) The 38 day old microbial mat prior to desiccation. (B) Desiccated microbial mat showing an irregular cracking pattern that is characterized by shallow, but wide radiating cracks. (C) Cracks continue to develop over the next 24 h. Coiling of the margins is increased and the cracks have merged further to produce composite pockets of cracks. Since curling of the margins obscured the original cracking pattern, it is highlighted by black lines. Note that the bottom left corner of the biomat remains mostly uncracked. The underlying sub-sediment shows no cracking, but has a pitted texture. (D) Desiccated abiotic, very fine sand substratum produced minor, thin cracks. Scale bar is 5 cm.

the biomat samples from both of these biotic experiments were covered by a cohesive layer of filamentous cyanobacteria characterized by elongated, segmented, tube-like bodies about 1 μm in diameter and over 50 μm long, and viscous EPS which coated cyanobacteria and the sediment (Fig. 9A, D).

A cross-sectional view shows that the cyanobacteria formed a dense 10 μm biomat (dry) on top of the sediment surface, but filaments and EPS penetrated into the pore spaces coating the grains with EPS and entangling the grains with filaments (Fig. 9B, E). In the very fine sand sediment, the cyanobacteria and EPS penetrated as deep as 500 μm into the sediment (Fig. 9B), while the cyanobacteria and EPS only penetrated about 150 μm into the clay-rich sediment (Fig. 9E). Cyanobacteria and EPS were scarce on the underside of the biomat curl structures (Fig. 9 C, F).

4. Discussion

4.1. Mechanisms behind crack formation

Shrinkage cracks develop when the stress induced from volume loss exceeds the tensile strength of that material (e.g., Bradley, 1933; Groisman and Kaplan, 1994; Shorlin et al., 2000). In the case of desiccation cracks, volume reduction is due to water loss. With microbially stabilized sediments, cracks can form abiotically (due to sediment shrinkage) or biotically (due to biomat shrinkage). The main observed factors that influenced cracking patterns in our experiments include, the thickness and vertical distribution of the shrinkage-prone materials (i.e. clay minerals or biomat) and physical heterogeneities therein.

4.1.1. Abiotic

The three abiotic sedimentary substrata produced cracks which are distinct from one another, because different grain sizes intrinsically possess characteristic crack-formation patterns. Flake-like clay particles were rearranged and brought closer together by capillary pressures, whereas rigid, spherical sand particles shrink very little with water loss (Bradley, 1933; Eriksson et al., 2007b). As expected, the homogeneous, clay-rich sediments were prone to deep, orthogonal cracking, while clean sand was not prone to cracking, except for minor, thin cracks that can be attributed to residual clay (Figs. 4D, 5D, 6D).

In the normally graded, clay-rich sediment the clay was increasingly abundant towards the top of the bed, which means that shrinking intensity of the sediment increased towards the bed-top (Fig. 6), resulting in raised crack-polygon margins (concave upwards crack polygons) (Bradley, 1933). In the ungraded, mixed clay-rich sediment, desiccation produced flat laying crack polygons, because clay was distributed evenly throughout the thickness of the sediment (Fig. 5). Therefore, the sediment experienced similar shrinkage rates throughout the bed thickness (Bradley, 1933).

In hypersaline lagoons, salt crystal precipitation due to evaporation may have effects similar to those described by Bradley (1933). The larger salt crystals that form on top of the finer clay particles, produce inverse grading that prevents curling of crack margins or even enables

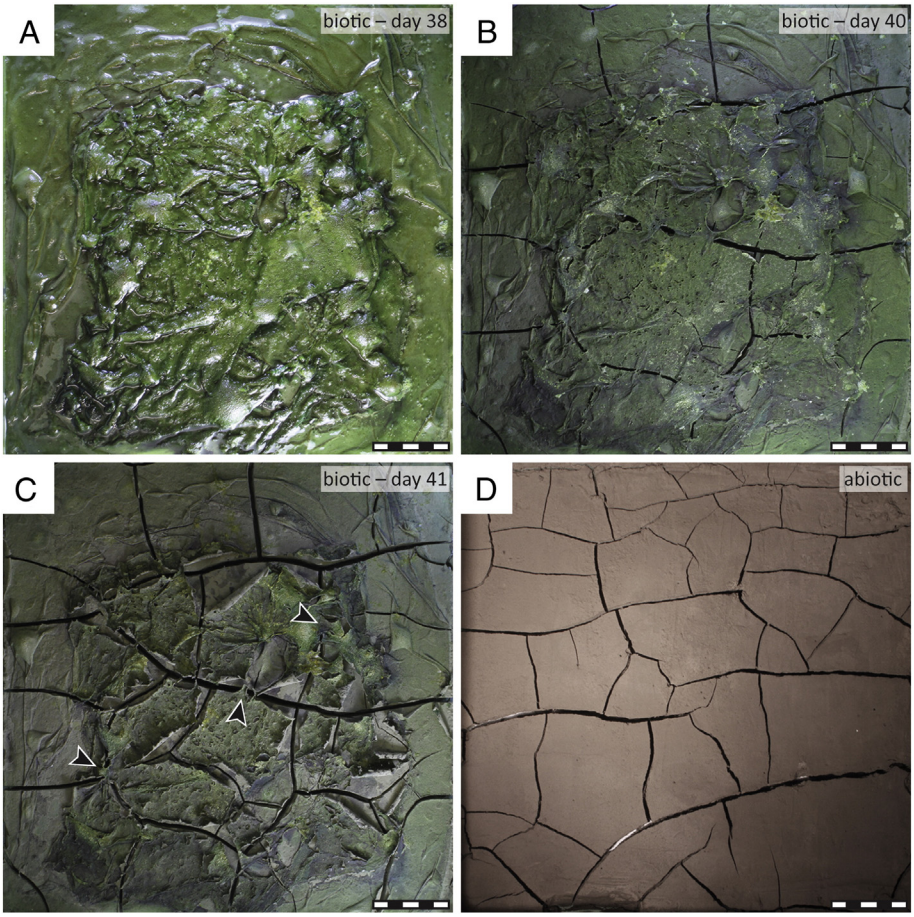

Fig. 5. Progressive desiccation of the biomat colonized mixed (ungraded) silt/clay (A–C) and desiccated abiotic mixed (ungraded) silt/clay substrata (D). (A) The 38 day old microbial mat prior to desiccation. Microbial mat is the thickest (oldest) at the center of the tank and becomes thinner (younger) towards the edges. (B) Clay desiccation preceded microbial mat desiccation, where the clay shrinkage rips the still moist microbial mat producing deep cracks. Microbial mat shows the ability to withstand crack propagation. (C) 24 h later, the desiccated microbial mat curls up at the existing crack margins, but also forms shallow cracks that are independent of the sub-sediment. The coiled crack margins were limited to the center of the tank where the older microbial mat desiccated. The younger 2 week old biofilm at the edges was not thick enough to curl. Intact microbial mat covers (bridges) some of the clay cracks even after drying (black arrows). (D) Desiccated abiotic mixed (ungraded) silt/clay substratum produces a regular network of cracks intersecting in 90–120° junctions forming detached crack-bound polygons. Scale bar is 5 cm.

convex crack margins that curl inward. Since deionized water was used in these abiotic experiments, there was no visible evaporite precipitation associated with desiccation.

4.1.2. Biotic

As observed under SEM, the topmost portions of the biomat consist of densely intertwined filaments and EPS (Fig. 9). Underneath the main biomat structure, filaments and EPS thrive in the pore spaces, but their abundance decreases with depth due to photosynthetic and metabolic limitations. In natural settings the uppermost microbial community traps and binds grains or is covered by accumulating sediment. In response, the cyanobacteria move upwards to re-establish themselves as a biomat above the sediment. Underneath, the sediment becomes incorporated into the mat fabric (Gerdes et al., 1993), similar to that observed in our experiments.

The water-rich biomat matrix shrunk substantially upon dehydration, bringing the entangled sediment grains into a closer packed arrangement, offering an alternative mechanism for desiccation crack formation. The ability of the uppermost biomat to contract with desiccation is much greater than the sediment below, thus at a certain depth there is a sharp (rather than gradational) change in the physical shear forces of the sediment. Desiccation results in the formation of coiled crack margins (mat curls), where the highly contracted, dry biomat and microbially bound sediment layer become separated from the more rigid sub-sediment below.

In our experiments, the desiccated mat curls were much thicker in the sand (Fig. 4C), as compared to the clay-rich sediment (Figs. 5C, 6C), due to a deeper colonization of the sand substratum. Thicker mats can be established on porous media, especially quartz-rich sediments that allows deeper light penetration (Gerdes, 2007). These experiments show that the thickness of the biomat had to be significant for the biotic cracks to develop: experiments using <20 day old biofilm did not develop mat curls, even though the sediment surface was covered with a film of cyanobacteria and EPS.

In nature, biomats are thicker stratified communities, where the top few millimeters are largely composed of photoauthotrophs and sulfur-oxidizing bacteria, while the deeper layers below light penetration are composed of various chemoheterotrophic bacteria (see Konhauser, 2007 for details). The biomats may also be vertically discontinuous, due to the repetitive burial by detritus or mineral precipitates (Cameron et al., 1985). Higher curled margins are observed to form in thicker biomats, where the curl height reaches over 3 cm in desiccating mat-sediment laminae that are 1.5–2.5 cm thick (Bose and Chafetz, 2009).

Coiled crack margins are one of the most notable indicators of biomat desiccation. This is not a unique property of the biomats, as swelling clays such as smectite are capable of producing similar coiled margins (Beraldi-Campesi and Garcia-Pichel, 2011). However, it was shown that the clay content has to be quite high in order for such curls to form: >30% smectite and >40% kaolinite. Only desiccation of

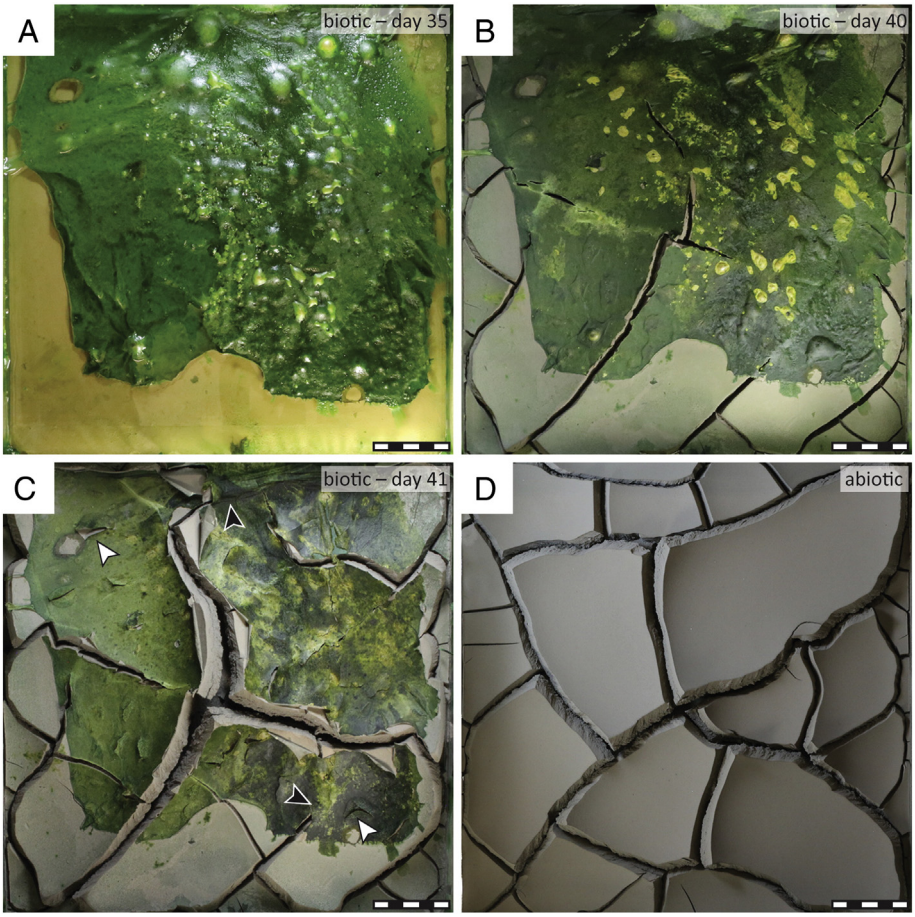

Fig. 6. Progressive desiccation of the biomat colonized normally graded silt/clay (A-C) and desiccated abiotic normally graded silt/clay substrata (D). (A) The 35 day old microbial mat prior to desiccation. (B) Clay desiccation preceded microbial mat desiccation and the clay-induced cracks rip the still moist microbial mat. (C) 24 h later, the desiccated microbial mat curls up at the existing crack margins. Dried gas domes became loci of shallow triradiate cracks (white arrows). Microbial mat bridges some of the clay cracks after drying (black arrows). (D) Desiccated abiotic normally graded silt/clay sediment produced a regular network of cracks connecting in 90–120° junctions forming detached crack polygons. Note the concave-up crack polygons in both biotic and abiotic substrata, due to the normal grading of the clay-rich sediment. Scale bar is 5 cm.

smectite results in coiled margins similar to mat curls seen in desiccating biomats (Beraldi-Campesi and Garcia-Pichel, 2011). Also, flip-overs and roll-up structures that are deformational features produced by shear stress acting on a biostabilized bedding plane, have a similar appearance to desiccation mat curls and may be easily misinterpreted in the rock record (Hagadorn and McDowell, 2012).

Salt encrustation in biostabilized sediments may subdue the curling of the margins, similar to the effect observed in abiotic sediment (Bradley, 1933), although it is noted that very abrupt normal grading that results in highly coiled crack margins cannot be easily inverted with salt precipitation. In carbonate settings, crack polygon margins have less developed curled margins, due to early carbonate precipitation (Bose and Chafetz, 2012). Perhaps salt encrustation in highly saline, evaporating conditions would have a similar effect.

4.2. Influence of biomats on desiccation crack development and resulting pattern

4.2.1. Cracks in sand substratum

Since the biomat is the only crack forming component in the clean sand, the produced crack pattern is solely controlled by shrinkage of the biomat, where the loci, distribution and propagation of cracks are controlled by regions of higher and lower tensile strength. The latter are ultimately related to mat growth and damage. Thus, fossil, as well as modern microbial desiccation cracks formed in sandy substrata, may have the following characteristics: (1) cracks that radiate from a point of weakness, resulting in pockets of composite radiate (often triradiate) cracks that do not connect to one another; (2) evidence of an irregular and incomplete crack network that produces connected (rather than detached) crack polygons; (3) cracks that are unusually wide (often as wide as they are long) due to coiling of the margins and evidence of the curled crack margins either preserved *in situ* or as mat chips; and (4) shallow cracks limited by the biomat thickness, while sediment underneath shows no cracking, and only an irregular, pitted pattern.

4.2.2. Cracks in clay-rich substratum

In the clay-rich sediments, the limited vertical distribution of the biomat rendered it subordinate to clay as the crack-forming mechanism. The desiccation of biostabilized clay-rich sediment resulted in two cracking patterns superimposed on one another: (1) prominent, deep cracks caused by the shrinkage of the clay; and (2) shallow, wide cracks caused by shrinkage of the biomat. These cracking patterns were not completely independent of each another as clay shrinkage, which occurred first, ripped areas of the thinner biomat creating loci for mat cracks. By contrast, the thicker, more cohesive biomat resisted tearing and bridged the clay-induced cracks, interfering with the abiotic crack pattern (Figs. 5, 6).

It was observed that biomats play a secondary role in crack formation in clay-rich substrata, thus cracks in such sediments are not solely due to microbial shrinkage. Microbial influence on cracking, however, can still be recognized as biostabilized clay-rich sediments have cracks

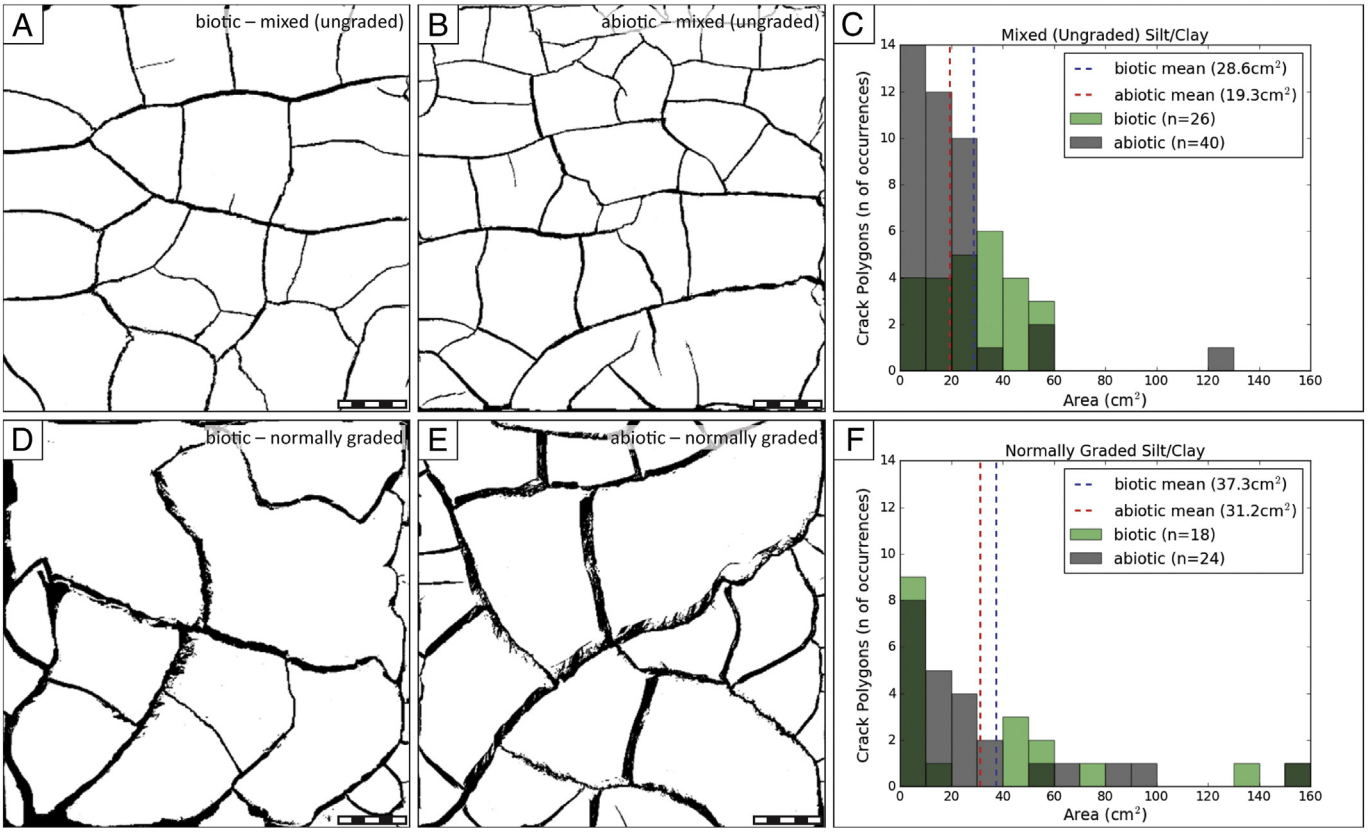

Fig. 7. Quantitative comparison of the biotic and abiotic crack-bound polygons formed in clay-rich substrata. (A, B) Binary images of the desiccated biotic and abiotic mixed (ungraded) silt/clay sediment, respectively. Black pixels represent cracks and white pixels represent crack polygons. (C) Surface areas of crack polygons formed in the mixed (ungraded) sediment are plotted as a histogram. The mean surface area of the biotic and abiotic crack polygons are 28.6 cm^2 and 19.3 cm^2, respectively. In the biotic sediment 26 crack polygons were identified, while in the abiotic sediment 40 crack polygons were identified. (D, E) Binary images of the desiccated biotic and abiotic normally graded silt/clay sediment, respectively. (F) Surface areas of crack polygons formed in the normally graded silt/clay sediment are plotted as a histogram. The mean surface area of the biotic and abiotic crack polygons are 37.3 cm^2 and 31.2 cm^2, respectively. In the biotic sediment 18 crack polygons were identified, while in the abiotic sediment 24 crack polygons were identified. Scale bar is 5 cm.

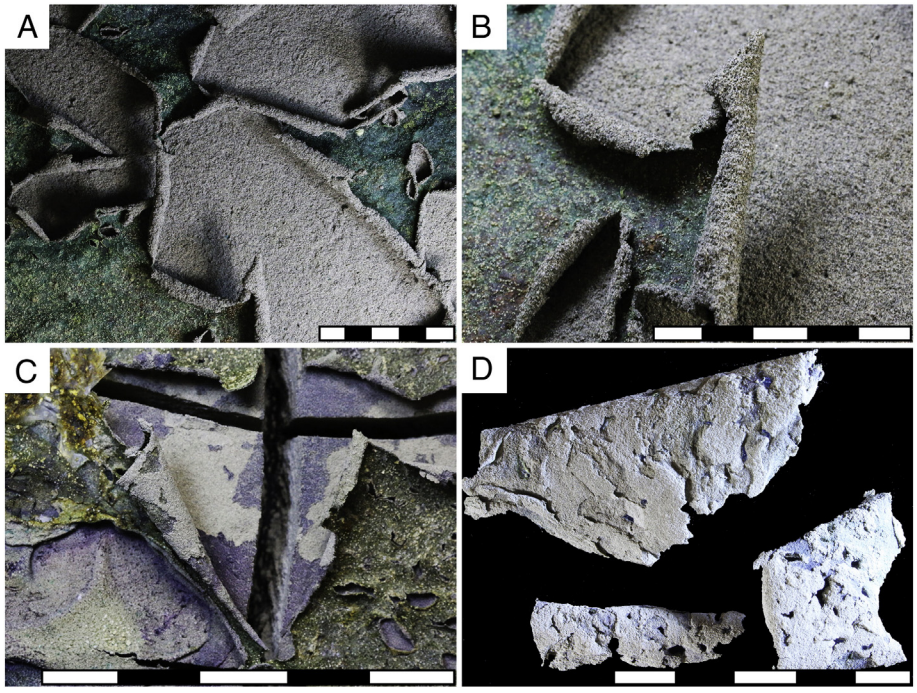

Fig. 8. Light macrographs of the microbial mat curls and textures left in the underlying sub-sediment. (A) Close-up image showing wide, but shallow cracks formed in the very fine sand substratum. Note the pitted texture that is left behind in the sub-sediment after detachment of the mat. (B) Coiled margins observed in the desiccated biomat and pitted texture in the sandy sub-sediment. (C) Deep clay-induced cracks, coiled crack margins and uneven, rugged texture observed in the mixed (ungraded) silt/clay sediment. (D) Rugged texture is also preserved on the underside of the mat curl structure. Scale bar is 5 cm.

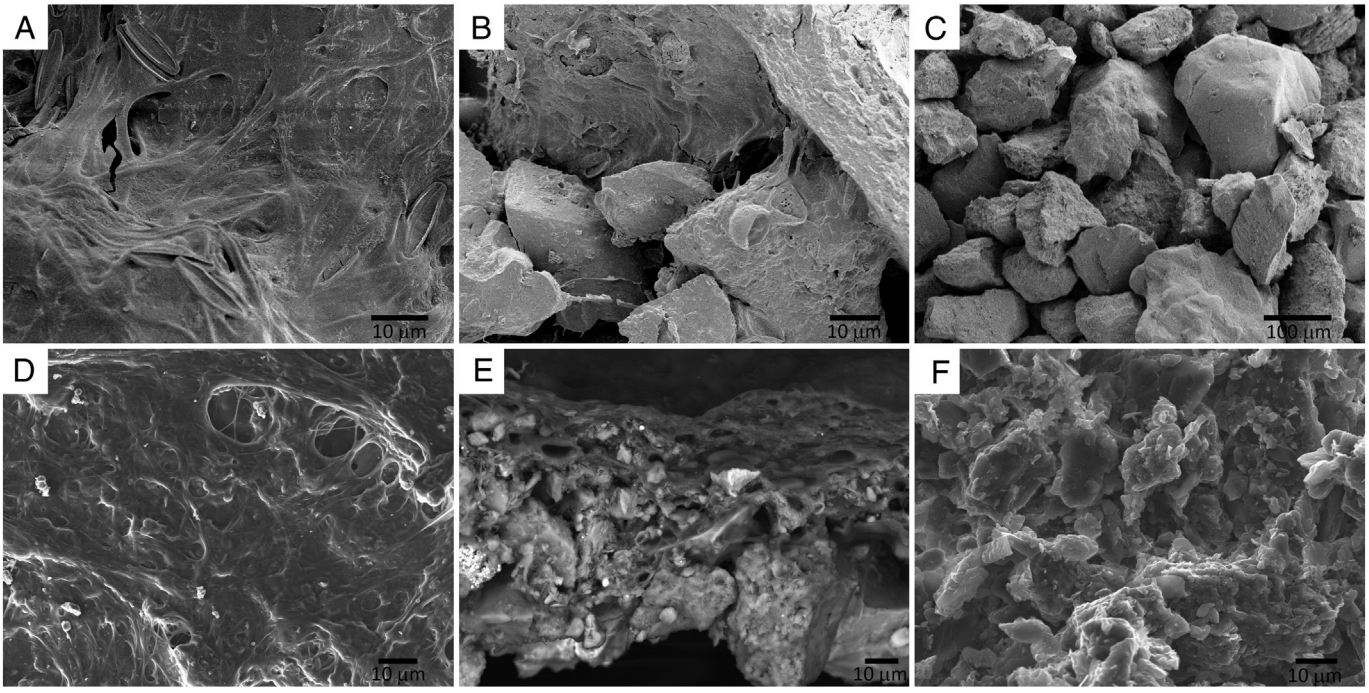

Fig. 9. SEM micrographs of the dry mat curls formed in the biostabilized very fine sand and mixed (ungraded) silt/clay sediment. (A) Plan view of the biostabilized very fine sand showing densely intertwined filamentous cyanobacteria and EPS. (B) Cross-sectional view of the dense microbial mat (top right corner) and penetration of cyanobacteria and EPS into the pore spaces between the sand grains. (C) View of the underside of the mat curl structure formed in the very fine sand, showing rare presence of cyanobacteria and EPS. (D) Plan view of the biostabilized mixed (ungraded) silt/clay sediment showing densely intertwined filaments and EPS, similar to that observed in the sand. (E) Cross-sectional view of the microbial mat and the microbially bound grains developed in the mixed (ungraded) silt/clay sediment. The bacteria and EPS do not penetrate as deeply into the clay-rich sediment as into the sand. (F) View of the underside of the curl structure formed in the mixed (ungraded) silt/clay sediment, showing rare presence of filaments and EPS.

that differ markedly from abiotic desiccation cracks and are characterized by: (1) overall deep polygonal crack network that is incomplete or irregular due to biomat bridging and inhibition of crack propagation, particularly if the abiotic cracking is not in line with biomat's own structural weaknesses and strengths; (2) crack polygons that are larger than expected considering the thickness of the cracked bed; and (3) evidence of a secondary shallow crack pattern that shows characteristics of the biomat desiccation described above from the sand-biomat substratum.

The crack-bound polygons in the biostabilized clay-rich sediment (both the mixed (ungraded) and normally graded silt/clay) were on average larger than in the abiotic sediment and less crack polygons formed in the biotic sediment as compared to the abiotic counterpart (Fig. 7). The observations are not unusual, as the study done by Bose and Chafetz (2009), showed that crack polygons which are formed in the biostabilized clay-rich sediment of Texas coast tidal flats, reached up to 50 cm in diameter, while the desiccated layer is no thicker than few centimetres. In homogeneous, abiotic sediments, crack polygon size typically increases with thickness of the bed (Plummer and Gostin, 1981), but the cohesive biomat cover subdues crack initiation as well as propagation. The reluctance of biomats to crack is also observed in the biostabilized sand substratum, where large areas of the desiccated biomat remained un-cracked, although show an overall shrinkage (i.e. reduction in surface area) (Fig. 4 C).

4.3. Comparison to the modern day and fossil microbial cracks

Curled crack margins, wide cracks and irregular networks match well with the general physiology of the cracks produced in modern subaerially exposed microbial mats, especially those formed in temporary pools where evaporation drives desiccation. Clay deposition can be common in such low energy settings and we suspect that clay shrinkage plays the primary role in the resulting polygonal network. The biomat retains moisture longer and plays an important secondary role by interfering with the clay-induced cracking, producing irregularities in the network and curled crack margins. Even though the preservation potential of such features is low, especially *in situ* preservation of the mat curls, Eriksson et al. (2000) provide fossil examples of interdune roll-up structures in the 1.8 Ga Waterberg Group fine-grained siliciclastic strata. More commonly the curled crack margins are broken off and transported/deposited elsewhere, producing “mat chips” (Pflüger and Gresse, 1996; Eriksson et al., 2007a).

Cracks formed in modern interdidal and supratidal settings are more variable, although are generally polygonal (Gerdes et al., 1993, 2000; Gerdes, 2007; Bose and Chafetz, 2009), even those formed in sandy (clay-poor) biostabilized sediment (Cameron et al., 1985). The polygonal pattern may be the result of a thicker desiccating biostabilized layer, where the bacteria penetrate deeper into the sediment, as compared to our experimental biomat, or because the entrapped or underlying clay fraction is high enough to play a role in crack initiation and distribution. Unfortunately the effect of clay on desiccation is not discussed while describing modern microbial cracks formed in the shrinking “mat-sediment laminae” (Bose and Chafetz, 2009) or simply desiccating “microbial mats” (Gerdes et al., 1993, 2000; Gerdes, 2007). Importantly, cracks that are observed in tidal settings may start out as uplifted petee ridges or gas domes, which rapture with desiccation (Cuadrado et al., 2014). The morphology and distribution of such cracks would be controlled by gas/water overpressure from below or deformation due to wind or water friction and is different from simple evaporation.

It is proposed that microbial mat genesis can only be accurately ascribed to fossil cracks if they are observed in clean (clay-free) sand (Eriksson et al., 2007a). While fossil “sand cracks” resemble microbial desiccation cracks in a sense that they are polygonal or triradiate (Eriksson et al., 2007a). Moreover many of the cracks tend to be narrow, aligned or overlapping, resembling synaeresis cracks (Porada and Loeffler, 2000; Bouougri and Porada, 2002; Parizot et al., 2005; Bouougri and Porada, 2007; Harazim et al., 2013). Disconnected, narrow cracks can be explained as incipient cracks that formed during initial stages of desiccation, whereas overlapping cracks should be explained

as multiple desiccation and biostabilization events that produce compound generations of cracks. Ability of the biomat to overgrow desiccation cracks was shown to increase their preservation potential and prevent healing during subsequent flooding, allowing the features to survive multiple dry/wet cycles (Gerdes et al., 1993; Gerdes, 2007).

Some authors argue that desiccation struggles to explain the diversity of fossil cracks and facilitate alternative explanations, such as the cracks may have formed intrastratally, where the water is expelled from the water-rich microbial mats with burial and pressure from the overlying sediment (Plummer and Gostin, 1981; Gehling, 1999; Harazim et al., 2013). Another possibility is that such cracks are not produced by shrinkage, but instead are mechanical pull-apart structures formed in gelatinous biostabilized layers under heavy overburden (Pflüger, 1999). Unfortunately, mechanisms of subaqueous and intrastratal crack formation are not that well known, but the differentiation of those and desiccation cracks is important and as such more research on this topic is warranted.

5. Conclusion

Based on our experiments, we conclude that microbial influence on the formation of desiccation cracks can be recognized in clean sand as well as clay-rich sediments. Because the biomat cannot penetrate deeply into clay-rich substrates, the influence of the former on fine-grained sediment is as a modifying agent of crack-margin and -morphology. In the sand, the biomat penetrates more deeply, forming discernible desiccation cracks, which do not form abiotically. Our work implies that biomats have two roles in the desiccation process depending on the substratum: (1) as the primary crack forming mechanism in sand; and (2) as a modifier of clay-induced cracks in clay-rich sediments. Key features of identifying a microbial influence on desiccation cracks in the rock record are limited, but include, disconnected, shallow, wide, radiating cracks which produce incomplete polygonal networks and different crack morphologies superimposed on each other.

Fossil microbial shrinkage cracks are identified as such, mainly based on evidence of biostabilization, rather than using the crack morphology itself. Fossil cracking patters are highly variable and some of the characteristics can be linked to desiccation, while others still remain debated. This work provides new insights into the mechanisms underpinning desiccation cracks, and it aids in differentiating between desiccation cracks (i.e. subaerial exposure) and cracks formed by other mechanisms.

Acknowledgements

The authors would like to express their appreciation to the Natural Sciences and Engineering Research Council of Canada, which funded this research (grant No. ZA619 to Gingras); Nathan Gerein for helping with the SEM analysis; L. Jamie Robbins and Neil MacPherson for helping with laboratory equipment.

References

Beraldi-Campesi, H., Garcia-Pichel, F., 2011. The biogenicity of modern terrestrial roll-up structures and its significance for ancient life on land. Geobiology 9, 10–23.
Bosak, T., Bush, J.M., Flynn, M.R., Liang, B., Ono, S., Petroff, A.P., Sim, M.S., 2010. Formation and stability of oxygen-rich bubbles that shape photosynthetic mats. Geobiology 8, 45–55.
Bose, S., Chafetz, H.S., 2009. Topographic control on distribution of modern microbially induced sedimentary structures (MISS); a case study from Texas coast. Sediment. Geol. 213, 136–149.
Bose, S., Chafetz, H.S., 2012. Morphology and distribution of MISS; a comparison between modern siliciclastic and carbonate settings. Spec. Publ. Soc. Sediment. Geol. 101, 3–14.
Bottjer, D., Hagadorn, J.W., 2007. Mat Growth Features. In: Schieber, J., Bose, P.K., Eriksson, P.G., Banerjee, S., Altermann, W., Catuneanu, O. (Eds.), Atlas of Microbial Mat Features Preserved Within the Clastic Rock Record. Elsevier, pp. 53–71.
Bouougri, E., Porada, H., 2002. Mat-related sedimentary structures in Neoproterozoic peritidal passive margin deposits of the West African Craton (Anti-Atlas, Morocco). Sediment. Geol. 153, 85–105.
Bouougri, E., Porada, H., 2007. Mat-related features from the Neoproterozoic Tizi n-Taghatine group, Nnti-Atlas belt, Morocco. In: Schieber, J., Bose, P.K., Eriksson, P.G., Banerjee, S., Altermann, W., Catuneanu, O. (Eds.), Atlas of Microbial Mat Features Preserved Within the Clastic Rock Record. Elsevier, pp. 198–207.
Bradley, W.H., 1933. Factors that determine the curvature of mud-cracked layers. Am. J. Sci. 26, 55–71.
Cameron, B.W., Cameron, D., Jones, J.R., 1985. Modern algal mats in intertidal and supratidal quartz sands, northeastern Massachusetts, U.S.A. SEPM Spec. Publ. 35, 211–223.
Carmona, N., Bournod, C., Ponce, J.J., Cuadrado, D., 2012. The role of microbial mats in the preservation of bird footprints; a case study from the mesotidal Bahia Blanca Estuary (Argentina). Spec. Publ. Soc. Sediment. Geol. 101, 37–45.
Cuadrado, D.G., Perillo, G.E., Vitale, A.J., 2014. Modern microbial mats in siliciclastic tidal flats; evolution, structure and the role of hydrodynamics. Mar. Geol. 352, 367–380.
De Boer, P.L., 1981. Mechanical effects of micro-organisms on intertidal bedform migration. Sedimentology 28, 129–132.
Decho, A., 1990. Microbial exopolymer secretions in ocean environments - their role(s) in food webs and marine processes. Oceanogr. Mar. Biol. 28, 73–153.
Dornbos, S.Q., Noffke, N., Hagadorn, J.W., 2007. Mat-decay features. In: Schieber, J., Bose, P.K., Eriksson, P.G., Banerjee, S., Altermann, W., Catuneanu, O. (Eds.), Atlas of Microbial Mat Features Preserved Within the Clastic Rock Record. Elsevier, pp. 106–110.
Eriksson, P.G., Porada, H., Banerjee, S., Bouougri, E., Sarkar, S., Bumby, A.J., 2007a. Mat-destruction features. In: Schieber, J., Bose, P.K., Eriksson, P.G., Banerjee, S., Altermann, W., Catuneanu, O. (Eds.), Atlas of Microbial Mat Features Preserved Within the Clastic Rock Record. Elsevier, pp. 76–105.
Eriksson, P.G., Schieber, J., Bouougri, E., Gerdes, G., Porada, H., Banerjee, S., Bose, P.K., Sarkar, S., 2007b. Classification of structures left by microbial mats in their host sediments. In: Schieber, J., Bose, P.K., Eriksson, P.G., Banerjee, S., Altermann, W., Catuneanu, O. (Eds.), Atlas of Microbial Mat Features Preserved Within the Clastic Rock Record. Elsevier, pp. 39–52.
Eriksson, P.G., Simpson, E.L., Eriksson, K.A., Bumby, A.J., Steyn, G.L., Sarkar, S., 2000. Muddy roll-up structures in siliciclastic interdune beds of the c. 1.8 Ga Waterberg Group, South Africa. PALAIOS 15, 177–183.
Gehling, J.G., 1999. Microbial mats in terminal Proterozoic siliciclastics: Ediacaran death masks. PALAIOS 14, 40–57.
Gerdes, G., 2007. Structures left by modern microbial mats in their host sediments. In: Schieber, J., Bose, P.K., Eriksson, P.G., Banerjee, S., Altermann, W., Catuneanu, O. (Eds.), Atlas of Microbial Mat Features Preserved Within the Clastic Rock Record. Elsevier, pp. 5–38.
Gerdes, G., 2010. What are microbial mats? In: Seckbach, J., Oren, A. (Eds.), Microbial Mats. Modern and Ancient Microorganisms in Stratified Systems. Springer, Dordrecht, pp. 5–28
Gerdes, G., Claes, M., Dunajtschik-Piewak, K., Riege, H., Krumbein, W.E., Reineck, H.E., 1993. Contribution of microbial mats to sedimentary surface structures. Facies 29, 61–74.
Gerdes, G., Klenke, T., Noffke, N., 2000. Microbial signatures in peritidal siliciclastic sediments: a catalogue. Sedimentology 47, 279–308.
Gingras, M., Hagadorn, J.W., Seilacher, A., Lalonde, S.V., Pecoits, E., Petrash, D., Konhauser, K.O., 2011. Possible evolution of mobile animals in association with microbial mats. Nat. Geosci. 4, 372–375.
Groisman, A., Kaplan, E., 1994. An experimental study of cracking induced by desiccation. Europhysics 25, 415–420.
Hagadorn, J.W., McDowell, C., 2012. Microbial influence on erosion, grain transport and bedform genesis in sandy substrates under unidirectional flow. Sedimentology 5, 795–808.
Harazim, D., Callow, R.T., McIlroy, D., 2013. Microbial mats implicated in the generation of intrastratal shrinkage ('synaeresis') cracks. Sedimentology 60, 1621–1638.
Konhauser, K., 2007. Introduction to Geomicrobiology. Blackwell Pub, Malden, MA (425 pp.).
Krumbein, W.E., 1983. Stromatolites – the challenge of a term in space and time. Precambrian Res. 20, 493–531.
Krumbein, W.E., Brehm, U., Gorbushina, A.A., Levit, G., Palinska, K.A., 2003. Biofilm, biodictyon and biomat – biolaminites, oolites, stromatolites – geophysiology, global mechanism and parahistology. In: Krumbein, W.E., Paterson, D.M., Zavarzin, G.A. (Eds.), Fossil and Recent Biofilms. Kluwer, Dordrecht, pp. 1–27.
Noffke, N., 1998. Multidirected ripple marks rising from biological and sedimentological processes in modern lower supratidal deposits (Mellum Island, southern North Sea). Geology 26, 879–882.
Noffke, N., 1999. Erosional remnants and pockets evolving frombiotic–physical interactions in recent lower supratidal environment. Sediment. Geol. 123, 175–181.
Noffke, N., Beukes, N., Gutzmer, J., Hazen, R., 2006a. Spatial and temporal distribution of microbially induced sedimentary structures: a case study from siliciclastic storm deposits of the 2.9 Ga Witwatersrand Supergroup, South Africa. Precambrian Res. 146, 35–44.
Noffke, N., Christian, D., Wacey, D., Hazen, R.M., 2013. Microbially induced sedimentary structures recording an ancient ecosystem in the ca. 3.48 billion-year-old Dresser Formation, Pilbara, Western Australia. Astrobiology 13, 1103–1124.
Noffke, N., Eriksson, K.A., Hazen, R.M., Simpson, E.L., 2006b. A new window into Early Archean life: microbial mats in Earth's oldest siliciclastic tidal deposits (3.2 Ga Moodies Group, South Africa). Geology 34, 253–256.
Owttrim, G.W., 2012. RNA helicases in cyanobacteria: biochemical and molecular approaches. Methods Enzymol. 511, 385–403.
Parizot, M., Eriksson, P.G., Aifa, T., Sarkar, S., Banerjee, S., Catuneanu, O., Altermann, W., Bumby, A.J., Bordy, E.M., Rooy, J.L.V., Boshoff, A.J., 2005. Suspected microbial mat-related crack-like sedimentary structures in the Palaeoroterozoic Magaliesberg Formation sandstones, South Africa. Precambrian Res. 138, 274–296.

Pecoits, E., Konhauser, K.O., Aubet, N.R., Heaman, L.M., Veroslavsky, G., Stern, R.A., Gingras, M.K., 2012. Bilaterian burrows and grazing behavior at >585 million years ago. Science 336, 1693–1696.
Pflüger, F., 1999. Matground structures and redox facies. PALAIOS 14, 25–39.
Pflüger, F., Gresse, P.G., 1996. Microbial sand chips — a non-actualistic sedimentary structure. Sediment. Geol. 102, 263–274.
Plummer, P.S., Gostin, V.A., 1981. Shrinkage cracks: desiccation or synaeresis? J. Sediment. Petrol. 51, 1147–1156.
Porada, H., Druschel, G., 2010. Evidence for participation of microbial mats in the deposition of the siliciclastic 'ore formation' in the Copperbelt of Zambia. J. Afr. Earth Sci. 58, 427–444.
Porada, H., Loeffler, T., 2000. Microbial shrinkage cracks in siliciclastic rocks of the Neoproterozoic Nosib Group (Damara Supergroup) of central Namibia. Commun. Geol. Surv. South West Africa/Namibia 12, 63–72.
Porada, H., Bouougri, E.H., Ghergut, J., 2007. Hydraulic conditions and mat-related structures in tidal flats and coastal sabkhas. In: Schieber, J., Bose, P.K., Eriksson, P.G., Banerjee, S., Altermann, W., Catuneanu, O. (Eds.), Atlas of Microbial Mat Features Preserved Within the Clastic Rock Record. Elsevier, pp. 258–265.
Porada, H., Ghergut, J., Bouougri, E.H., 2008. Kinneyia-type wrinkle structures: critical review and model of formation. PALAIOS 23, 65–77.
Sarkar, S., Banerjee, S., Samanta, P., Jeevankumar, S., 2006. Microbial mat-induced sedimentary structures in siliciclastic sediments; examples from the 1.6 Ga Chorhat Sandstone, Vindhyan Supergroup, M. P., India. J. Earth Syst. Sci. 115, 49–60.
Sarkar, S., Bose, P.K., Samanta, P., Sengupta, P., Eriksson, P.G., 2008. Microbial mat mediated structures in the Ediacaran Sonia Sandstone, Rajasthan, India, and their implications for Proterozoic sedimentation. Precambrian Res. 162, 248–263.
Schieber, J., 1998. Possible indicators of microbial mat deposits in shales and sandstones; examples from the mid-Proterozoic Belt Supergroup, Montana, U.S.A. Sediment. Geol. 120, 105–124.
Schieber, J., Bose, P.K., Eriksson, P.G., Banerjee, S., Altermann, W., Catuneanu, O. (Eds.), 2007. Atlas of Microbial Mat Features Preserved Within the Clastic Rock Record. Elsevier, Amsterdam, Netherlands (324 pp.).
Seilacher, A., 1999. Biomat-related lifestyles in the Precambrian. PALAIOS 14, 86–93.
Seilacher, A., 2008. Biomats, biofilms, and bioglue as preservational agents for arthropod trackways. Palaeogeogr. Palaeoclimatol. Palaeoecol. 270, 252–257.
Shepard, R.N., Sumner, D.Y., 2010. Undirected motility of filamentous cyanobacteria produces reticulate mats. Geobiology 8, 179–190.
Shorlin, K.A., de Bruyn, J.R., Graham, M., Morris, S.W., 2000. Development and geometry of isotropic and directional shrinkage-crack patterns. Phys. Rev. E 61, 6950–6957.